A Letters Journal Exploring the Frontiers of Physics

September 2019

EPL, **127** (2019) 54002
doi: 10.1209/0295-5075/127/54002

www.epljournal.org

The collective behaviour of ensembles of condensing liquid drops on heterogeneous inclined substrates

Sebastian Engelnkemper[1] and Uwe Thiele[1,2,3(a)]

[1] *Institut für Theoretische Physik, Westfälische Wilhelms-Universität Münster - Wilhelm Klemm Str. 9, 48149 Münster, Germany*
[2] *Center of Nonlinear Science (CeNoS), Westfälische Wilhelms-Universität Münster - Corrensstr. 2, 48149 Münster, Germany*
[3] *Center for Multiscale Theory and Computation (CMTC), Westfälische Wilhelms-Universität - Corrensstr. 40, 48149 Münster, Germany*

received 26 January 2019; accepted in final form 3 September 2019
published online 16 October 2019

PACS 47.55.df – Drops and bubbles: Breakup and coalescence
PACS 47.20.Ky – Nonlinearity, bifurcation, and symmetry breaking
PACS 68.15.+e – Liquid thin films

Abstract – Employing a long-wave mesoscopic hydrodynamic model for the film height evolution we study ensembles of pinned and sliding drops of a volatile liquid that continuously condense onto a chemically heterogeneous inclined substrate. Our analysis combines, on the one hand, path continuation techniques to determine bifurcation diagrams for the depinning of single drops of nonvolatile liquid on single hydrophilic spots on a partially wettable substrate and, on the other hand, time simulations of growth and depinning of individual condensing drops as well as of the long-time behaviour of large ensembles of such drops. Pinned drops grow on the hydrophilic spots, depin and slide along the substrate while merging with other pinned drops and smaller drops that slide more slowly, and possibly undergo a pearling instability. As a result, the collective behaviour converges to a stationary state where condensation and outflow balance. The main features of the emerging drop size distribution can then be related to single-drop bifurcation diagrams.

Copyright © EPLA, 2019

Introduction. – The behaviour of liquid drops on solid homogeneous and heterogeneous substrates is of high relevance to many processes of everyday life and for technological processes such as printing, coating and cooling [1]. The behaviour of individual drops is frequently studied experimentally and theoretically, considering, *e.g.*, spreading and sitting drops without lateral driving [2], laterally driven drops, *e.g.*, by gravity on an incline, that are pinned by substrate heterogeneities [3,4] or freely slide along a homogeneous substrate [5,6]. However, in applications such as condensation or printing, one is often interested in the collective behaviour of large drop ensembles. This problem has attracted much interest in particular for rigid substrates where the interactions between individual drops and the resulting mass transfer processes determine the ensemble behaviour. The long-time merging within such drop ensembles is a particular soft matter example of a coarsening process similar to the Ostwald-ripening of crystalline nanoparticles [7], quantum dots [8] or emulsion droplets [9] where the mean drop/cluster/dot size and their mean distance continuously increase in time following power laws. For simple nonvolatile liquids on horizontal homogeneous substrates coarsening is well studied experimentally [10–12] and theoretically through simulations and asymptotic considerations [13–15] mainly based on thin-film (or lubrication or long-wave) equations with a mass-conserving dynamics [16–18]. Additionally including condensation, the process is also studied employing particle-based statistical models and Smoluchowski-type (cf. [19]) evolution equations for distribution functions of drop sizes [20]. With lateral driving forces, the dynamics of drop ensembles is dramatically different as the sliding speed of drops strongly depends on their size. The resulting relative motion of differently sized drops makes overall coarsening much faster than without lateral driving forces. However, instabilities may counteract coalescence and at large times the ensemble dynamics may self-organise and converge to an almost stationary drop

(a) E-mail: u.thiele@uni-muenster.de

size distribution [21]. Examples are drops that slide under an air flow or on an incline as well as spinodal decomposition under flow [22]. Here, we investigate the influence of substrate heterogeneities and continuous condensation on the dynamics of laterally driven drop ensembles. We establish the resulting basic features employing a long-wave model and the particular choice of randomly distributed identical heterogeneities. Note that condensing and coalescing drops with instantaneous sliding avalanches have also been described with particle-based statistical models and Smoluchowski-type equations [23].

More in detail, ref. [6] analyses a long-wave mesoscopic hydrodynamic model employing numerical path continuation techniques [24,25] and establishes the bifurcation behaviour of single sliding drops of nonvolatile liquid on smooth homogeneous inclined substrates. They find that at fixed lateral forcing [volume] beyond a critical volume [forcing] related to a saddle-node bifurcation and a nearby global bifurcation, sliding drops undergo a pearling instability [5] and emit satellite droplets at their back. Reference [6] also quantifies how sliding speed and the mentioned critical parameter values depend on drop size and driving strength. This allows one to characterise the fast coalescence of drops and the resulting fast coarsening under driving. In a multiscale approach, ref. [21] then connects the single-drop results with the time evolution of the drop size distribution obtained in large-scale direct numerical simulations (DNS) of drop ensembles and, in consequence, derives a Smoluchowski-type statistical model for the drop size distribution. Main features of the resulting steady distribution can be related to the bifurcation diagram of single sliding drops. The approach of refs. [6,21] is based on a number of strong assumptions that are difficult to realise in experiments as most real substrates are heterogeneous, the used liquids are often volatile and periodic boundary conditions are rather difficult to achieve for sliding drops under lateral driving. Here, we adapt their approach to more realistic experimental conditions.

In particular, first, we incorporate i) the deposition of liquid by condensation and ii) heterogeneous wettability in the form of hydrophilic spots into the long-wave thin-film model. Next, we follow the methodology outlined above: We employ continuation techniques to obtain the bifurcation diagram for the depinning behaviour of single drops of nonvolatile liquid. This is then compared with simulations of growth and depinning dynamics of single drops that condense onto single spots. Finally, the resulting bifurcation diagram is related to large-scale DNS and it is discussed how the existence of heterogeneities and liquid condensation affect the ensemble behaviour.

Modelling and numerical implementation. – We employ a nondimensional long-wave equation to model the time evolution of the height profile $h(x, y, t)$ that describes drops of a volatile liquid on a partially wetting, heterogeneous substrate, cf. [26,27] and references therein:

$$\partial_t h = -\nabla \cdot [Q(h)(\nabla p + \boldsymbol{\chi})] + \beta(p - \mu) \qquad (1)$$

with the pressure $p(x, y, t) = \Delta h + [1 + \xi g(x, y)]\Pi(h)$, where Δh and $\Pi(h) = -\partial_h f(h)$ are the Laplace and Derjaguin (or disjoining) pressure, respectively [2,28]. The latter results from the wetting energy $f(h) = -1/2h^2 + 1/5h^5$. Note that p may be expressed as variation of a free energy functional [29]. The function $\xi g(x, y)$ represents the heterogeneous wettability of the substrate, namely, the local long-wave equilibrium contact angle $\theta_{\mathrm{eq}}(x, y) \propto \sqrt{1 + \xi g(x, y)}$ while the scaled equilibrium adsorption layer height remains constant $h_0 = 1$. For drops on an incline, the driving force is given by $\boldsymbol{\chi} = G(\alpha, 0)^T$, where G is the gravitation number and α is the scaled inclination angle[1]. Here, the heterogeneities take the form of randomly distributed identical small circular hydrophilic regions, *i.e.*, more wettable spots, with a small continuous transition region towards the partially wetting background substrate. In particular, for a single spot we employ $g(\tilde{r}) = -\frac{1}{2}[\tanh(\tilde{r} + R) - \tanh(\tilde{r} - R)]$ with $\tilde{r}^2 = (x - x_i)^2 + (y - y_i)^2$, where R is the uniform spot radius and (x_i, y_i) the centre position of spot i. Furthermore, β is an evaporation rate and μ is the partial ambient vapour pressure. In combination they control the strength of condensation or evaporation. Note that the dependence on pressure automatically incorporates the Kelvin effect and a wettability-dependence of phase change —for a discussion of evaporation models see [30]. The model is analysed employing i) numerical pseudo-arclength path-continuation techniques [24,25] implemented using pde2path [31] and ii) direct numerical simulations (DNS) based on a finite-element method on a quadratic mesh with bilinear ansatz functions and a 2nd-order implicit Runge-Kutta scheme for time stepping implemented using the DUNE PDELab framework [32,33].

Single-drop depinning. – On a smooth homogeneous substrate, drops of any size slide for arbitrarily small lateral driving, *i.e.*, for any $\alpha \neq 0$ [6]. In stark contrast, on a heterogeneous substrate, drops are pinned at small driving strength as investigated in depth with long-wave models for drops on one-dimensional substrates [26,34] and on two-dimensional substrates with stripe-like heterogeneity [3,35]. Figure 1 presents for a single drop of nonvolatile liquid pinned by a single circular hydrophilic spot a typical bifurcation diagram at fixed drop volume V_{D} employing the driving strength α as control parameter (top)[2] and selected corresponding drop profiles (bottom).

[1] Starting from the dimensional Derjaguin pressure $\tilde{\Pi}(\tilde{h}) = -A/\tilde{h}^3 + B/\tilde{h}^6$, we scale height by $h_{\mathrm{eq}} = (B/A)^{1/3}$, lateral lengths by $l_0 = \sqrt{3}h_{\mathrm{eq}}/\sqrt{5}\theta_{\mathrm{eq}}$, and time by $t_0 = 9\eta h_{\mathrm{eq}}/25\gamma\theta_{\mathrm{eq}}^4$. Then, $\theta_{\mathrm{eq}} = \sqrt{3A/5\gamma h_{\mathrm{eq}}^2}$ is the equilibrium contact angle at $\xi = 0$ and $G = 3\rho g h_{\mathrm{eq}}^2/5\gamma\theta_{\mathrm{eq}}^2$ is the gravitation number. The physical inclination angle is $\theta_{\mathrm{eq}}\alpha$. Here, we use $G = 10^{-3}$, *e.g.*, for $\theta_{\mathrm{eq}} = 0.1$, h_{eq} is about a micron. We do not expect qualitative changes for smaller h_{eq} [6] —a case that is at present not numerically feasible.

[2] As solution measure we mainly use the L^2-norm $\|\delta h\| := \sqrt{\Omega^{-1}\int_\Omega [h/h_0 - 1]^2 \mathrm{d}x\mathrm{d}y}$. Spherical cap-like drops of large volume are characterised by a relatively large $\|\delta h\|$, which is reduced for

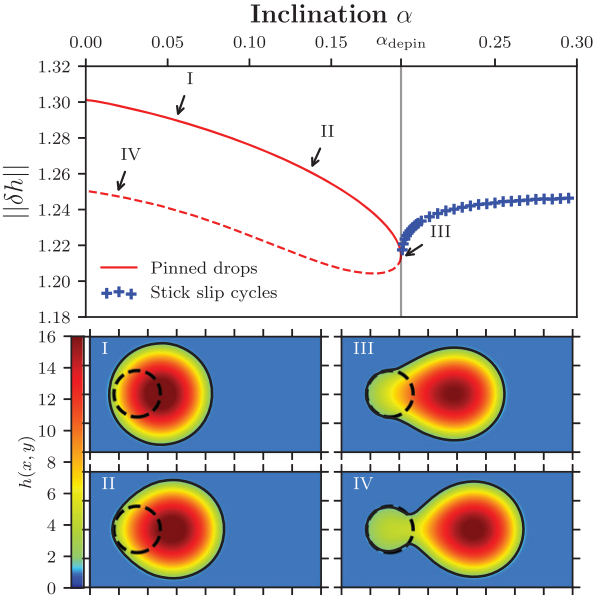

Fig. 1: Typical bifurcation diagram (top) and selected drop profiles as contour plots (bottom) related to the depinning of a drop of partially wetting, nonvolatile ($\beta = 0$) liquid from a circular hydrophilic spot (dashed lines in bottom panels) under lateral driving. The bifurcation diagram gives the (time-averaged) L^2-norm $\|\delta h\|$ as a function of substrate inclination α (*i.e.*, strength of driving) for linearly stable and unstable pinned drops (solid and dashed line, respectively) and for the depinned sliding drops that undergo a periodic stick-slip motion in the considered periodic setting (cross symbols). The parameters of the drop profiles are indicated by corresponding roman numbers in the upper panel. The domain size is $l_x \times l_y = 200 \times 100$ and $\xi = 1.0$, the drop volume is fixed at $V_{\mathrm{D}} = 5 \times 10^4$ and the spot radius is $R = 20$.

Further cases are discussed in the Supplementary Material `Supplementarymaterial.pdf` (SM). At small driving there exists a branch of linearly stable pinned drops sitting off-centre on the spot (*e.g.*, I, II) and a branch of unstable drops that are located slightly downstream of the spot and connect to it by a narrow liquid bridge (*e.g.*, IV). Starting from a spherical cap-like drop at $\alpha = 0$ (not shown), with increasing α the stable drop first keeps its spherical cap-like shape but shifts its centre downstream (I). Further increasing α, the drop is increasingly deformed, so that $\|\delta h\|$ decreases monotonically (II). The branch of linearly stable states ends in a saddle-node bifurcation at $\alpha_{\mathrm{depin}} \approx 0.1926$ (III) where it annihilates with the branch of unstable states. As known from other geometries [3,34], at the saddle-node bifurcation a branch of stick-slip states emerges in a global bifurcation. As here we work with periodic boundary conditions, these represent time-periodic states with a period that diverges when approaching the bifurcation point.

drops that are small or strongly deformed. The drop volume V_{D} is measured as the volume above the adsorption layer of height $h_0 = 1$.

Each cycle of the resulting motion has two distinct phases: first, the drop is pinned by the spot but slowly stretches downstream. Then it depins and slides fast to the next defect where it pins again. This is illustrated in the SM. Close to the bifurcation, the time scales for the stick- and the slide-phase strongly differ, and the overall behaviour closely resembles experimentally observed stick-slip motion [4]. Note, that the unstable steady states represent critical perturbations that have to be overcome to depin and start to slide already below the critical driving strength, *i.e.*, for $\alpha < \alpha_{\mathrm{depin}}$.

Single-drop condensation and depinning. – Next we introduce condensation ($\beta > 0$ and $\mu < 0$ in eq. (1)). Then, on the partially wettable background substrate the equilibrium adsorption layer height is only slightly shifted (given by $\Pi(h) - \mu = 0$), but on the hydrophilic spots, the film height grows with a rate $|\beta\mu|$ (marginally slowed down by the Kelvin effect). As a result, individual drops condense onto the hydrophilic substrate defects. As their mass continuously grows, they eventually reach the critical mass for depinning at fixed inclination and depin under the influence of the lateral driving force. After depinning, drops slide and may undergo a pearling instability similar to ref. [21].

We first quantify this process and its dependence on condensation rate in fig. 2 for a single drop on a hydrophilic spot. The figure compares the bifurcation curve of steady pinned drops as a function of their volume V_{D} (at fixed inclination) with the time evolution of condensing drops for two different condensation rates. Note, that in contrast to fig. 1 periodic boundary conditions (BC) are only used in the spanwise (*i.e.*, y-) direction, while in streamwise (*i.e.*, x-) direction Neumann BC are used. At the upstream border the film is always flat and Neumann BC result in no-flux BC while downstream these BC allow drops to slide out of the domain. The same BC are employed in the ensemble DNS below.

Here, each time simulation is started from a flat film of adsorption layer height $h_0 = 1$, *i.e.*, $V_{\mathrm{D}} = 0$ and $\|\delta h\| = 0$. Subsequently, liquid condenses into a drop on the ideally wettable spot. As soon as the height profile deviates from a flat film, a finite Laplace pressure results in a slight decrease (increase) of condensation in the bulk drop (contact line) region. This results in further small internal fluxes that rearrange liquid within the drops.

Inspecting the top panel of fig. 2 in detail, one appreciates that the growing drops (*e.g.*, bottom panels II and III) closely follow in the $(V_{\mathrm{D}}, \|\delta h\|)$-plane the bifurcation curve representing stable steady drops of different volumes. This holds up to the saddle-node bifurcation that indicates depinning for drops of nonvolatile liquids. The slightly smaller norm at identical volume indicates a smaller contact angle —an effect that is more pronounced at larger condensation rates, *i.e.*, at larger deviation from equilibrium. For evaporating drops, it is known that due to evaporation-driven internal flows towards the contact

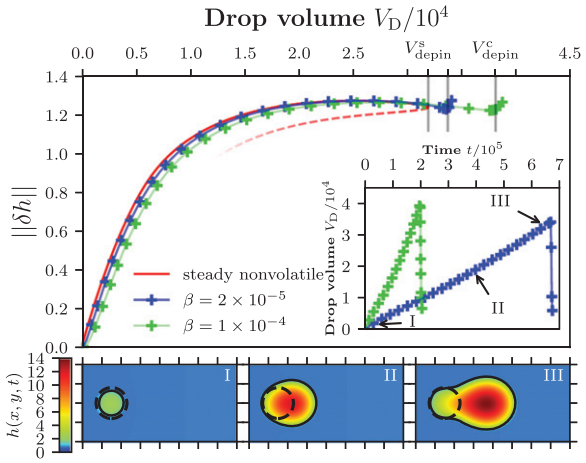

Fig. 2: Top: the lines with symbols characterise the time evolution of a single drop of volatile liquid that grows by condensation on a hydrophilic spot. Shown is the L^2-norm $\|\delta h\|$ over drop volume V_D for two different condensation rates as given in the legend and for comparison the bifurcation curve of pinned nonvolatile drops (bare solid line). The short vertical lines indicate the volume at depinning in the nonvolatile (V^s_{depin}, left line) and volatile (V^c_{depin}, right lines) case. The inset gives $V_D(t)$ for the condensing drops. The bottom row gives snapshots of the growing pinned drop for $\beta = 2 \times 10^{-5}$ at times marked by roman numbers in the inset. The domain size is $l_x \times l_y = 200 \times 100$, $\xi = 1.0$, the inclination is fixed at $\alpha = 0.3$, the spot radius is $R = 20$ and the partial vapour pressure that drives condensation is $\mu = -0.05$.

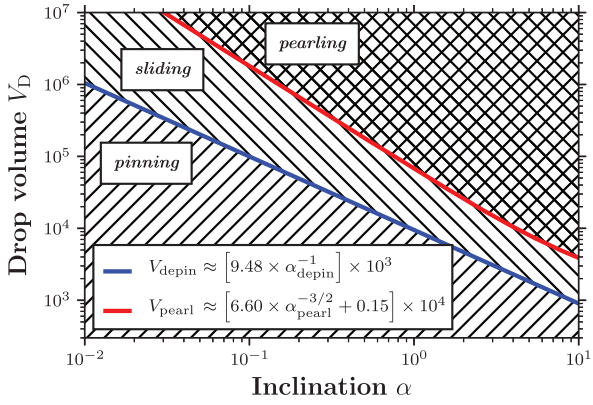

Fig. 3: Morphological phase diagram in the nonvolatile case indicating where pinned, stable sliding and pearling drops dominate in the parameter plane spanned by drop volume and inclination angle. The borders between regions correspond to power laws (given in the inset) extracted from sets of bifurcation diagrams as, *e.g.*, fig. 1 above and fig. 1 of [6]. Remaining parameters are as in fig. 1.

line region, the contact angle is larger than the equilibrium value [27,36]. Here, we encounter the expected opposite effect for condensing drops due to condensation-driven internal flows towards the drop centre.

When the drops pass the critical volume for depinning $V^s_{depin} \approx 3.19 \times 10^4$ of the steady nonvolatile drop, they depin. However, with ongoing condensation, the volume where this happens is moderately shifted to a larger V^c_{depin} (in fig. 1 indicated by the two short vertical lines on the right) because the time scale of the depinning process has to become shorter than the one for condensation. Therefore the shift $V^c_{depin} - V^s_{depin}$ is larger for faster condensation (larger β). After the connection to the defect is capped, at the present moderate lateral driving the sliding drop closely approaches a slightly oval spherical cap-like shape (small but distinct increase of the norm close to V^c_{depin}). The sliding drop moves downstream and quickly leaves the domain. This results in the abrupt decrease in volume visible in the inset of fig. 2. As the qualitative behaviour is similar for all considered condensation rates, now we focus on the larger one ($\beta = 10^{-4}$) as this allows for large-scale DNS on time scales that are large as compared to time scales of condensation, depinning and sliding.

If the domain is sufficiently extended, at high driving strength one can observe that the drop undergoes a pearling instability (as in ref. [6]). As in the following, depinning and pearling will play an important role, we present in fig. 3 a morphological phase diagram for single drops in the nonvolatile case. It indicates in a log-log plot volume and inclination ranges where drops are pinned at the defect, slide down the homogeneous background substrate and undergo a pearling instability while sliding. The separating lines can be fitted by the power laws given in the legend of fig. 3.

Large-scale time simulation. – Large-scale DNS of eq. (1) are conducted on a large spatial domain (4000×4000) with about 400 identical randomly distributed, not overlapping, hydrophilic spots of radius $R = 20$ (see black spots in the top left panel of fig. 4) for different fixed inclination angles. We believe this relatively high spot density presents a good first approximation for a heterogeneous substrate. Note that at this density most drops will interact with several defects before leaving the domain. This also ensures that the results will not critically depend on streamwise domain size as may be the case at low spot density.

Statistical analyses are applied to the resulting ensembles of growing pinned and sliding drops[3]. To shorten the initial transient, here, the initial condition is a flat film of height $h_{ini} = 2.0$ perturbed by small-amplitude additive noise and a further spatial harmonic modulation of large wavelength. The latter induces different initial conditions (IC) at the individual hydrophilic spots, so that artificially synchronised behaviour is avoided and the system

[3]To quantify the process, the total number of drops $N_D(t)$ in the domain is determined as well as all individual drop volumes and the resulting drop size distribution $f(V_D, t)$. We define an individual drop via the connected area A_D of its footprint where the height $h(x, y, t)$ is larger than a threshold height that is slightly larger than the height of the adsorption layer (here $h_{thresh} = 1.05$). For each step of the DNS, all drop volumes V_D are calculated by integrating $h(x, y, t)$ over the corresponding A_D. Then the distribution $f(V_D, t)$ is obtained by a Gaussian kernel density estimate (KDE) [37].

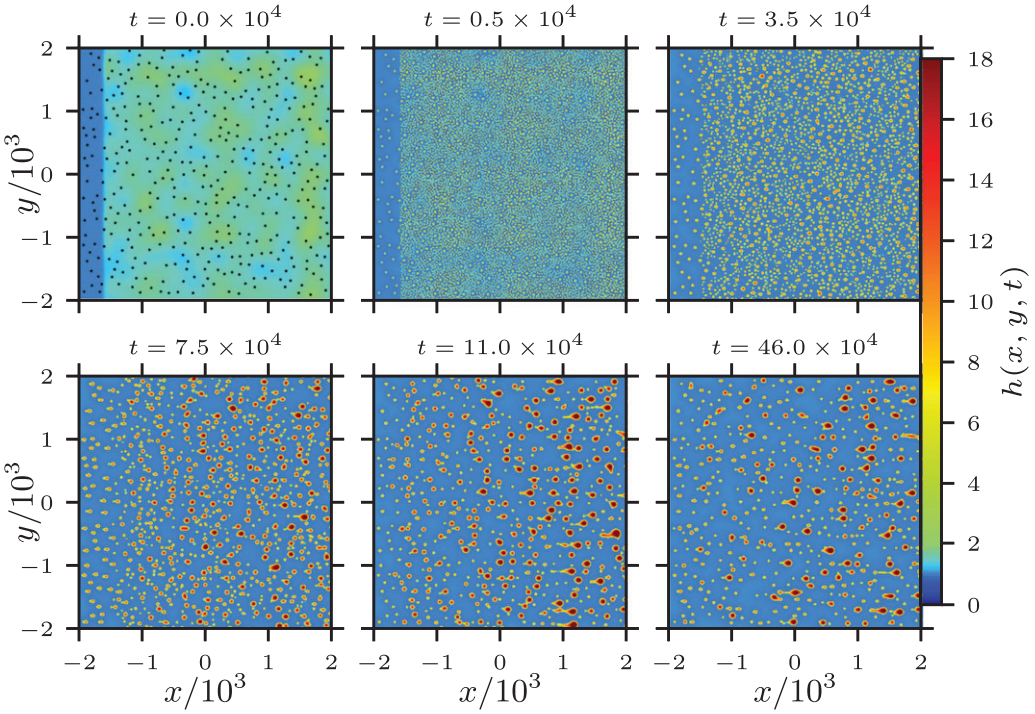

Fig. 4: Shown are snapshots from a large-scale direct time simulation (eq. (1)) of an ensemble of condensing drops on an inclined substrate with $N_S \approx 400$ identical randomly distributed hydrophilic spots with $R = 20$ (black dots in top left panel). The condensation rate is moderate $\beta = 10^{-4}$, $\alpha = 0.5$, and the domain size is 4000×4000. During an initial transient, spinodal dewetting contributes to the formation of drops that later (from about $t = 10^4$) mainly condense onto the hydrophilic spots. From $t \approx 7.5 \times 10^4$ the dynamics is dominated by pinned and sliding drops. In the long-time limit (here, reached at $t \approx 25 \times 10^4$) the dynamics converges to a stationary state where condensation, depinning and inclination-driven outflow balance, resulting in a steady drop size distribution.

sufficiently fast approaches a purely statistical state. Furthermore, at the upstream boundary a strip of bare adsorption layer height is introduced into the IC to ensure the no-flux BC (fig. 4 (top left)). In this way, the total volume in the domain exclusively results from a balance of condensation and downstream outflow.

The series of snapshots in fig. 4 presents important phases of the resulting dynamics for $\alpha = 0.5$. A comparison with other inclinations is given in the SM. The corresponding dependencies of mean film height $\bar{h}$ and drop number N_D on time are given in fig. 5. The first phase (top row of fig. 4) represents a transient dominated by spinodal dewetting that results in the fast emergence of many small droplets and their subsequent coarsening (decrease of N_D in fig. 5) accompanied by an ongoing increase of $\bar{h}$ due to condensation. The effect of the hydrophilic spots is clearly visible at $t = 0.5 \times 10^4$ (fig. 4) where significantly larger droplets have developed on all of them. They absorb the smaller droplets within their immediate vicinity and attract most condensation. The remaining small droplets continue their coarsening and fusion into the large drops at the defects. A clear qualitative difference is seen in the transition from $t = 3.5 \times 10^4$ to $t = 7.5 \times 10^4$ as most droplets from initial dewetting have disappeared and the dynamics is dominated by condensation and depinning. At $t \approx 10^5$ the decreasing N_D is converging to a steady

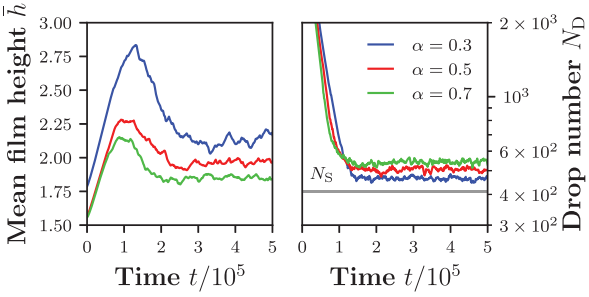

Fig. 5: Time evolution of (left) the mean film height $\bar{h}$ and (right) the drop number N_D obtained in large-scale DNS at different inclinations α as given in the legend. The number N_S of hydrophilic spots is shown as thin horizontal line. In all cases, first ($t \lesssim 10^5$) condensation, spinodal dewetting and drop coarsening dominate, *i.e.*, $\bar{h}$ increases and N_D decreases. Then depinned drops slide out of the domain and $\bar{h}$ decreases, until at about $t = 2, \ldots, 3 \times 10^5$ a balance of condensation and outflow is established. With decreasing α, the stationary state is characterised by a smaller N_D and a larger $\bar{h}$.

number while $\bar{h}$ still decreases due to the outflow of the initial batch of larger drops.

At large times (*e.g.*, $t = 46.0 \times 10^4$ in fig. 4) a steady drop size distribution has developed where N_D and $\bar{h}$ fluctuate about their respective mean values. This implies that

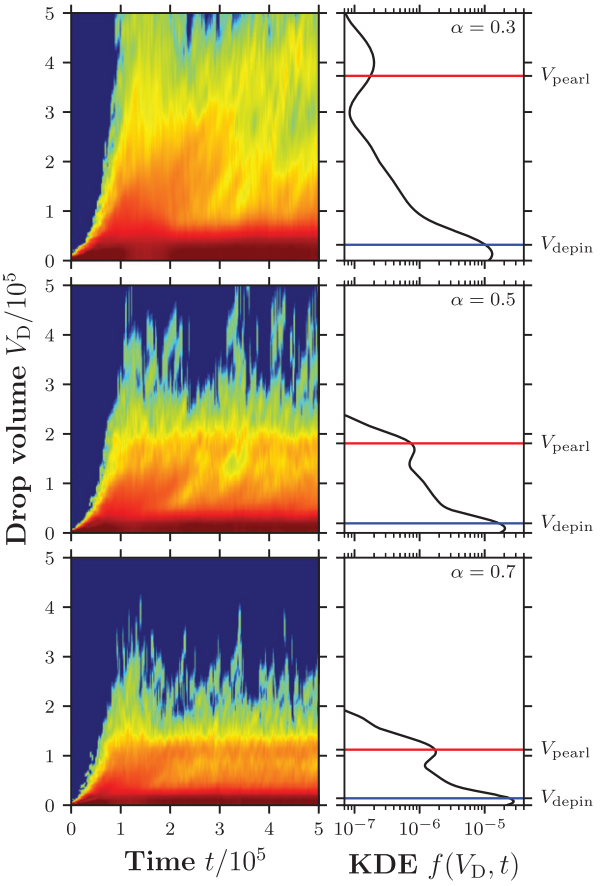

Fig. 6: The left panels show time evolutions of the drop size distribution as volume-time plots of the Gaussian kernel density estimate (KDE) $f(V_D, t)$ for (top) $\alpha = 0.3$, (middle) $\alpha = 0.5$ and (bottom) $\alpha = 0.7$. The phases described at fig. 5 can be well distinguished. The respective right panels give the final steady drop size distributions $f(V_D)$, obtained as time average of the converged but fluctuating distribution from $t = 4.5 \times 10^5$ to $t = 5.0 \times 10^5$. The critical drop sizes for depinning V_{depin} and pearling V_{pearl} are indicated as horizontal lines (cf. fig. 3).

condensation and outflux balance in a stationary state. Thereby, the values of the corresponding plateaus in fig. 5 for N_D ($\bar{h}$) decrease (increase) with increasing inclination: At low α, the depinning threshold V_{depin} is larger than at high α, and the ensemble consists of fewer and larger drops (for an image see SM). In all cases, the number of hydrophilic spots N_S naturally forms the lower limit for N_D, such that $N_D - N_S$ indicates the number of sliding drops. Due to later depinning and slower sliding the mean height in the domain is larger at lower α. It is notable that here N_D truly converges in the long time limit while in the nonvolatile case on homogeneous substrates the drop number still slowly decreases in the long-time limit [21]. There this small drift is due to large linearly stable sliding drops that feature a long backwards protrusion [6]. In the present case, such drops are disturbed and broken up by the heterogeneities.

Two further effects are visible in fig. 4: First, one discerns a gradient in drop sizes in streamwise direction which results from the increase of drop size as they move through the domain and collect liquid from hydrophilic spots that they pass. Second, in contrast to the homogeneous substrates [21], the ensemble always remains dominated by a large number of relatively small drops pinned at the hydrophilic spots. This is very clear in fig. 6 where on the left volume-time plots of the drop size distribution $f(V_D, t)$ are shown for different driving strength while on the right the resulting steady distributions $f(V_D)$ are shown. We always find that a characteristic double-peaked drop size distribution emerges. The loci of the two peaks are close to the critical drop sizes for depinning V_{depin} and pearling V_{pearl}, respectively, that are obtained from the single-drop bifurcation diagrams (figs. 1 and 3). With decreasing α the peaks become wider and their distance becomes larger. Notably, at low α an intermediate range between the peaks emerges where $f(V_D)$ decreases exponentially with increasing drop size.

Conclusion. – We have employed a long-wave film height evolution equation to qualitatively study the collective behaviour of ensembles of pinned and sliding drops of volatile liquid on chemically heterogeneous inclined substrates combining path-continuation methods and large-scale direct numerical simulations. We have obtained bifurcation diagrams that quantify the depinning of individual drops from hydrophilic spots in the nonvolatile case and could show that such a bifurcation curve roughly predicts the path taken by the continuous condensation of individual drops onto such spots. In the case of the drop ensemble condensing onto many identical randomly distributed, not overlapping, hydrophilic spots, beyond depinning the drops slide along the substrate, collect the liquid of other pinned drops and of smaller drops that slide more slowly. Sufficiently large sliding drops undergo a pearling instability. We have found, that as a result of these competing processes the collective behaviour of the drop ensemble converges to a stationary state of on average balanced condensation and outflow. The stationary state is characterized by a drop size distribution whose main features are related to the single-drop bifurcation diagrams.

In the future, it will be interesting to determine how the collective behaviour depends on details of the wetting behaviour, on the parameters related to condensation and on the characteristics of the substrate heterogeneities. Of particular interest are the spatial, size, shape and wettability distribution of the heterogeneities. Further it is of interest if the described features are robust beyond the long-wave approximation.

* * *

We acknowledge support by the German-Israeli Foundation for Scientific Research and Development (GIF,

Grant No. I-1361-401.10/2016) and by the Deutsche Forschungsgemeinschaft (DFG, Grant No. TH781/12 within SPP 2171).

REFERENCES

[1] de Gennes P.-G., Brochard-Wyart F. and Quéré D., *Capillarity and Wetting Phenomena: Drops, Bubbles, Pearls, Waves* (Springer, New York) 2004.
[2] de Gennes P.-G., *Rev. Mod. Phys.*, **57** (1985) 827.
[3] Beltrame P., Knobloch E., Hänggi P. and Thiele U., *Phys. Rev. E*, **83** (2011) 016305.
[4] Varagnolo S., Ferraro D., Fantinel P., Pierno M., Mistura G., Amati G., Biferale L. and Sbragaglia M., *Phys. Rev. Lett.*, **111** (2013) 066101.
[5] Podgorski T., Flesselles J.-M. and Limat L., *Phys. Rev. Lett.*, **87** (2001) 036102.
[6] Engelnkemper S., Wilczek M., Gurevich S. V. and Thiele U., *Phys. Rev. Fluids*, **1** (2016) 073901.
[7] Rinkel T., Nordmann J., Raj A. and Haase M., *Nanoscale*, **6** (2014) 14523.
[8] Vengrenovich R., Gudyma Y. and Yarema S., *Semiconductors*, **35** (2001) 1378.
[9] Taylor P., *Adv. Colloid Interface Sci.*, **75** (1998) 107.
[10] Andrieu C., Beysens D. A., Nikolayev V. S. and Pomeau Y., *J. Fluid Mech.*, **453** (2002) 427.
[11] Blaschke J., Lapp T., Hof B. and Vollmer J., *Phys. Rev. Lett.*, **109** (2012) 068701.
[12] Baratian D., Dey R., Hoek H., van den Ende D. and Mugele F., *Phys. Rev. Lett.*, **120** (2018) 214502.
[13] Gratton M. and Witelski T., *Physica D*, **238** (2009) 2380.
[14] Glasner K., Otto F., Rump T. and Slepcev D., *Eur. J. Appl. Math.*, **20** (2009) 1.
[15] Kitavtsev G. and Wagner B., *J. Eng. Math.*, **66** (2010) 271.
[16] Oron A., Davis S. H. and Bankoff S. G., *Rev. Mod. Phys.*, **69** (1997) 931.
[17] Craster R. V. and Matar O. K., *Rev. Mod. Phys.*, **81** (2009) 1131.
[18] Thiele U., *J. Phys.: Condens. Matter*, **22** (2010) 084019.
[19] Smoluchowski M. V., *Z. Phys.*, **17** (1916) 557.
[20] Meakin P., *Rep. Progr. Phys.*, **55** (1992) 157.
[21] Wilczek M., Tewes W., Engelnkemper S., Gurevich S. V. and Thiele U., *Phys. Rev. Lett.*, **119** (2017) 204501.
[22] He D. Q. W. and Nauman E. B., *Chem. Eng. Sci.*, **52** (1997) 481.
[23] Cheng Z., Redner S., Meakin P. and Family F., *Phys. Rev. A*, **40** (1989) 5922.
[24] Dijkstra H. A., Wubs F. W., Cliffe A. K., Doedel E., Dragomirescu I. F., Eckhardt B., Gelfgat A. Y., Hazel A., Lucarini V., Salinger A. G., Phipps E. T., Sanchez-Umbria J., Schuttelaars H., Tuckerman L. S. and Thiele U., *Commun. Comput. Phys.*, **15** (2014) 1.
[25] Engelnkemper S., Gurevich S., Uecker H., Wetzel D. and Thiele U., *Computational Modeling of Bifurcations and Instabilities in Fluid Mechanics*, *Computational Methods in Applied Sciences*, Vol. **50** (Springer) 2019, Chapt. "Continuation for thin film hydrodynamics and related scalar problems", pp. 459–501.
[26] Thiele U. and Knobloch E., *New J. Phys.*, **8** (2006) 313.
[27] Todorova D., Thiele U. and Pismen L. M., *J. Eng. Math.*, **73** (2012) 17.
[28] Starov V. M. and Velarde M. G., *J. Phys.: Condens. Matter*, **21** (2009) 464121.
[29] Thiele U., *Colloids Surf. A*, **553** (2018) 487.
[30] Thiele U., *Adv. Colloid Interface Sci.*, **206** (2014) 399.
[31] Uecker H., Wetzel D. and Rademacher J., *Numer. Math.-Theory Methods Appl.*, **7** (2014) 58.
[32] Bastian P., Blatt M., Dedner A., Engwer C., Klöfkorn R., Kornhuber R., Ohlberger M. and Sander O., *Computing*, **82** (2008) 103.
[33] Bastian P., Blatt M., Dedner A., Engwer C., Klöfkorn R., Kornhuber R., Ohlberger M. and Sander O., *Computing*, **82** (2008) 121.
[34] Thiele U. and Knobloch E., *Phys. Rev. Lett.*, **97** (2006) 204501.
[35] Beltrame P., Hänggi P. and Thiele U., *EPL*, **86** (2009) 24006.
[36] Morris S. J. S., *J. Fluid Mech.*, **432** (2001) 1.
[37] Scott D. W., *Multivariate Density Estimation: Theory, Practice, and Visualization*, 2nd edition (John Wiley & Sons, Hoboken, NJ) 2015.